Nanobody Mediated Macromolecular Crowding Induces Membrane Fission and Remodeling in the African Trypanosome

Authors: Alexander Hempelmann[1], Laura Hartleb[2], Monique van Straaten[1], Hamidreza Hashemi[3], Johan P. Zeelen[1], F. Nina Papavasiliou[3], Markus Engstler[2], C. Erec Stebbins[1†], and Nicola G. Jones[2†]

Affiliations:

[1]Division of Structural Biology of Infection and Immunity, German Cancer Research Center, Heidelberg, Germany.

[2]Department of Cell and Developmental Biology, Theodor-Boveri-Institute, Biocenter, University of Würzburg, Würzburg, Germany.

[3]Division of Immune Diversity, German Cancer Research Center, Heidelberg, Germany.

[†]Correspondence to: nicola.jones@uni-wuerzburg.de, e.stebbins@dkfz-heidelberg.de

The dense Variant Surface Glycoprotein (VSG) coat of African trypanosomes represents the primary host-pathogen interface. Antigenic variation prevents clearing of the pathogen by employing a large repertoire of antigenically distinct VSG genes, thus neutralizing the host's antibody response. To explore the epitope space of VSGs, we generated anti-VSG nanobodies and combined high-resolution structural analysis of VSG-nanobody complexes with binding assays on living cells, revealing that these camelid antibodies bind deeply inside the coat. One nanobody caused rapid loss of cellular motility, possibly due to blockage of VSG mobility on the coat, whose rapid endo- and exocytosis is mechanistically linked to *T. brucei* propulsion and whose density is required for survival. Electron microscopy studies demonstrated that this loss of motility was accompanied by rapid formation and shedding of nanovesicles and nanotubes, suggesting that increased protein crowding on the dense membrane can be a driving force for membrane fission in living cells.

Keywords

African Trypanosome, Host-Pathogen Interaction, Variant Surface Glycoproteins, Immune Epitope Mapping, Structural Biology, Nanovesicle Formation, Nanotube Formation, Protein Crowding, Membrane Fission

Introduction

Trypanosoma brucei and related parasites cause African sleeping sickness in humans and Nagana in cattle. A distinguishing feature of these pathogens is a densely packed surface coat that is populated almost entirely by the **V**ariant **S**urface **G**lycoprotein (**VSG**) in the mammalian-infectious forms of the parasite. As *T. brucei* is an extracellular pathogen, the VSG coat is extensively exposed to the immune system and is the primary surface of interaction within the host. It is also highly antigenic, leading quickly to robust antibody mediated responses that are neutralizing (Borst, 2002; Overath et al., 1994). However, parasites possess an extensive genetic repertoire of antigenically distinct VSGs (2000+ genes and pseudogenes), allowing individual parasites to switch the coat to another variant, thus creating a novel surface array to which the immune system is naïve and must readapt. This process of antigenic variation repeats with recurring cycles of parasite clearance, coat switching, and pathogen regrowth (Bangs, 2018).

In addition to antigenic variation, trypanosomes employ another immune evasion mechanism, antibody clearance and subsequent recycling of VSG molecules. This process helps evasion of complement-mediated immune destruction but is only effective at low antibody titer (Engstler et al., 2007; Horn, 2014; Mugnier et al., 2016; Pal et al., 2003). Facilitated by the remarkably high endocytosis rate at the flagellar pocket, anti-VSG antibodies are selectively removed from VSG molecules within minutes (Engstler et al., 2004; Webster et al., 1990). This requires high mobility of the VSG molecules and free lateral diffusion (Bülow et al., 1988; Hartel et al., 2016, 2015).

The VSGs are glycosylated, homodimeric proteins of roughly 60 kDa comprised of two subdomains: a long, rod-like N-terminal domain (NTD) spanning approximately 350 amino acids followed by a C-terminal domain (CTD) of roughly 100 amino acids that attaches to the

57 glycophosphatidylinositol (GPI) anchor which links the protein to the membrane. The antigenic
58 region of the protein is considered to be the NTD and, in particular, the upper regions of the NTD
59 that would be exposed to the immune system in the dense packing of tens of millions of VSG
60 proteins on the surface (Schwede et al., 2015). The NTDs are composed of a tightly packed three-
61 helix-bundle decorated with extended insertions that produce top and bottom "lobes" at polar ends
62 of the rod-like, helical scaffolding.

63 Despite decades of research, very little is known about the interactions of immune proteins
64 with the VSG coat. Few studies have mapped any defined natural epitopes and at present no
65 antibody-VSG co-crystal structures exist. Reviewing multiple indirect studies (involving
66 monoclonal antibodies, nanobodies, polyclonal antisera, lectins, and proteases), Schwede et al.
67 propose that contrary to many discussions in published literature, a substantial portion of the N-
68 terminal domain (ending at the bottom lobe) of the VSGs could be accessible to the immune system
69 (Schwede et al., 2015).

70 In order to address this topic, we pursued structural studies of several camelid nanobodies
71 raised to the VSG coat. These provide both a biologically relevant context (as *T. brucei* related
72 species cause surra in camelids – (Radwanska et al., 2018)), as well as a system generally amenable
73 to crystallographic analysis (de Marco, 2011). While camels and llamas have a very similar
74 immune system to humans and rodents, there are variations. Nanobodies (Nbs) are single chain,
75 minimal variable region-containing antibody fragments consisting of one protein domain. They
76 tend to be highly stable and to crystallize very well and thus are useful alternatives to studying
77 pathogen-immune interactions if the larger mouse and human antibodies are challenging to
78 crystallize.

79 Previous studies have shown that high-affinity Nbs can be effectively raised to VSGs (Arbabi-
80 Ghahroudi, 2017). Addition of such Nbs to AnTat1.1 expressing *T. brucei* was shown to induce
81 trypanosome lysis even in the absence of the effector Fc domain (Stijlemans et al., 2017). This
82 effect was described to initiate quick immobilization of trypanosomes, enlargement of the flagellar
83 pocket and a major blockage of endocytosis. However, the mechanism mediating these phenomena
84 have remained obscure.

85 In this study, we used the camelid immune system (Figure S1) to generate a series of
86 nanobodies to *T. brucei* VSG2 (also known as VSG221 or VSG MITat1.2). X-ray crystallographic
87 studies reveal that these nanobodies bind not to the upper, exposed surface of the elongated VSG
88 molecules, but instead as much as 100 Å from the top. Indeed, we find that these nanobodies and
89 their corresponding camelid antibodies are also able to recognize the intact trypanosome coat on
90 living cells. These results demonstrate that VSG epitopes buried deeply in the dense surface coat
91 are in fact accessible to B-cells and secreted antibodies.

92 Similar to prior reports, this binding can be highly toxic to the parasite (Stijlemans et al., 2011,
93 2017) and we observed paralysis of the normally highly mobile trypanosomes within minutes of
94 nanobody addition. This paralysis was linked to a nanobody induced block on VSG diffusion in
95 the coat. Parasite movement and endo- and exocytosis of the coat are mechanistically linked and
96 essential for survival in the mammalian host. At the same time, VSG density on the coat is highly
97 regulated, and significant raising of the density adversely impacts VSG movement in the
98 membrane (Hartel et al., 2016), making the African trypanosome a unique model system for
99 studying the effects of protein crowding in living cells. Examination of the parasite by electron
100 microscopy after Nb binding demonstrated that loss of VSG mobility (and subsequent loss of
101 cellular motility) was accompanied by rapid formation and shedding of nanovesicles and

102 nanotubes, suggesting that increased protein crowding on this already dense membrane physically
103 drives membrane fission – the first example of this phenomenon in living cells.

104

105 **Results**

106 **Production and Crystal Structures of VSG2-Nanobody Complexes**

107 Nanobodies were generated from llamas immunized with the N-terminal domain of VSG2
108 (Methods). To ensure that the clones were able to bind within surface coats and not only the soluble
109 form of the VSG, a filtering step of panning the library of B-cell clones against intact UV-
110 inactivated trypanosomes was added and all clones were scored by flow cytometry analysis as
111 binding to intact, live trypanosomes. From this we obtained a library of 69 distinct nanobodies
112 (belonging to 30 different CDR3 groups or B-cell lineages). We initially crystallized three different
113 clones complexed to VSG2 ($NB9_{VSG2}$, $NB11_{VSG2}$, and $NB14_{VSG2}$, Figure 1, Methods, Figure S2,
114 Table S1 and S2). Those structures revealed that all the nanobodies bound similarly to the same
115 epitope region and possessed a highly conserved consensus set of amino acids in the CDR1 and
116 CDR3 loops that characterized the majority of clones in the library, despite being derived from
117 independent B-cell lineages (discussed below). To identify other binding modalities, we searched
118 for clones in our library with the most divergent CDR regions. A few such were identified, and we
119 crystallized one of these ($NB19_{VSG2}$) which indeed bound in a distinct location on VSG2. However,
120 unexpectedly, this was not on the top, putative antigenic surface of the molecule, but nearly 100 Å
121 down from the upper surface at the bottom of the N-terminal domain and adjacent to the postulated
122 location of the CTD (Bartossek et al., 2017). The overall structure of VSG2 is not significantly
123 changed from that previously reported (Freymann et al., 1990), aligning with a root-mean-square-
124 deviation in 1440 atomic positions of 0.5 Å (single monomer).

125 **Nanobodies Bind Deep into the VSG Coat**

126 Three of the nanobodies ($NB9_{VSG2}$, $NB11_{VSG2}$, and $NB14_{VSG2}$) bind in an identical position.
127 The binding site is approximately 60 Å down from the upper lobe of VSG2 and formed by a
128 concave surface on the VSG 3-helix bundle about midway down the length of the rod-like NTD
129 (Figure 1A and B). This is consistent with a hypothesis that nanobodies are more likely to bind
130 concave or convex surfaces than flat ones (Stijlemans et al., 2004). Numerous side chains from the
131 second two helices of the helical bundle make contacts to the nanobodies (residues spanning 100-
132 115 and 280-302 of VSG2), with the primary contacts solvent-facing, predominantly hydrophilic
133 residues (e.g. Q111, T112, A285, E286, T301, and D313) as well as several minor side chain
134 contacts and backbone contacts (Figure 2A). These nanobodies interact with VSG2 through their
135 variable CDR1 and CDR3 loops (without any significant contacts from the CDR2 loop) with a
136 consensus set of side chains (CDR1 residues T28, S30, N31 and CDR3 residues L100, L101, S103,
137 Figure 2, A and C). In contrast, $NB19_{VSG2}$ binds underneath the bottom lobe of VSG2 purely
138 through CDR3 (Figure 2B). The contacts are a mixture of hydrophobic and polar interactions, but
139 with a preponderance of aromatic side chain stacking (π-stacking) interactions involving residues
140 W102, W112, and Y115 of $NB19_{VSG2}$ with the side chains Y375 and Y376 of VSG2.

141 **Nanobody Binding is Detectable on Living Parasites**

142 In order to examine the physiological relevance of these nanobodies and their unexpected
143 binding sites on VSG2, we performed a series of binding experiments to living trypanosomes.
144 Nanobodies harboring a C-terminal hexa-histidine (6xHis) tag were added to trypanosomes
145 expressing different VSGs and the cells analyzed with an anti-tag monoclonal antibody by
146 fluorescence-activated cell sorting (FACS, Methods, Figure 3). Nanobodies $NB9_{VSG2}$, $NB11_{VSG2}$,
147 and $NB14_{VSG2}$ were easily detected as binding to VSG2 expressing cells with several logs

148 difference in signal (Figure 3A), whereas nanobody NB19$_{VSG2}$ could not be detected. In contrast,
149 nanobodies did not bind other VSGs (Figure 3, B-D), thereby showing high specificity (NB11$_{VSG2}$
150 shown as an example). Verifying that the surface accessibility is not only limited to the relatively
151 small nanobodies, we created a sortaggable variant of the camelid heavy chain IgG2 antibody with
152 the corresponding NB11$_{VSG2}$ Ig domain and found it can, in fact, bind the live parasite coat (Figure
153 S3A).

154 The inability to detect NB19$_{VSG2}$ raised the possibility that the binding we observed in solution
155 and in the crystal structure was an artifact of using the soluble VSG2 as the antigen for
156 immunization. A second possibility was that the deep binding we observe in the crystal structure
157 buries NB19$_{VSG2}$ beyond the reach of IgG antibodies. To distinguish between these two models,
158 we directly labeled NB19$_{VSG2}$ and other nanobodies with fluorescent moieties. In one case we
159 chemically conjugated the fluorophore FITC to the proteins (to free amine groups, typically
160 exposed lysine residues), showing that the nanobodies generally could be detected and also how
161 they compare to a full anti-VSG2 IgG (Figure 3E). While a small shift in fluorescence intensity
162 can be observed for NB19$_{VSG2}$-FITC (compared to the non-stained sample, Supplementary Figure
163 3F), it showed significance in 2-tailed t-test ($p= 0.0109$, Supplementary Figure 3M). To further
164 probe binding, we sought to avoid whole-scale labeling of proteins chemically, and turned to a
165 single, site-specific covalent modification of the Nbs (Figure 3F, Methods). Here, we used the
166 transpeptidase enzyme sortase to attach peptide-linked 6-Carboxyfluorescein (FAM) to the C-
167 terminus of the nanobodies (Methods). In this case, all nanobodies showed binding to the living
168 trypanosomes, although NB19$_{VSG2}$ and NB9$_{VSG2}$ seem to have reduced relative fluorescence
169 intensity (yet with signal intensity over negative controls, Figure 3F). To buttress the positive
170 binding result for NB19$_{VSG2}$ by a third independent experiment, we also exposed living

171 trypanosomes to the nanobodies, thoroughly washed the cells, and then probed them by Western
172 blot (Figure 3G). All the nanobodies, including $NB19_{VSG2}$, were shown to have bound, whereas an
173 irrelevant nanobody raised to the *Helicobacter pylori* BabA antigen did not bind VSG2 expressing
174 trypanosomes.

175

176 **Probing Nb-VSG2 Interactions**

177 To further examine the interactions of the Nbs with VSG2, we created mutations in the
178 consensus site of CDR3 of $NB11_{VSG2}$ and two critical contacts to VSG2 from $NB19_{VSG2}$ (Figure
179 4). We focused on these two because $NB11_{VSG2}$ possess a highly similar consensus binding site to
180 $NB9_{VSG2}$ and $NB14_{VSG2}$, whereas $NB19_{VSG2}$ differs in the binding location and in sequence to the
181 others. The alteration of these important contacts led to a disruption of binding to VSG2 as assayed
182 by gel filtration chromatography. In particular, even single loss-of-contact mutations to the
183 $NB19_{VSG2}$ interface completely disrupted binding, whereas it required a triple mutant in $NB11_{VSG2}$
184 to abrogate complex formation, suggesting that the complex was more stable (Figure 4).

185

186 **Nanobodies to VSG2 Reduce Coat Mobility, Cause Stiffening of the Cell Body and Stall**
187 **Parasite Motion**

188 As previous reports had shown Nb-induced interference with trypanosome movement (Stijlemans
189 et al., 2011), VSG2 expressing wild type cells were treated with saturating amounts of the four
190 nanobodies. Only treatment with $NB11_{VSG2}$ resulted in reduced cell motility (Figure S4). While at
191 5 min post addition of $NB11_{VSG2}$ swimming behavior of the parasites remained largely normal
192 with individual cells actively swimming and changing direction, from 15 min onwards, cell

193 movement was clearly affected as trajectories became shorter and mostly unidirectional (Figure
194 5A and Figure S4C). A closer inspection of these trajectories suggested that the parasites were not
195 motionless, but that translocation was largely due to drift in the sample which is unavoidable in
196 recordings of this duration. Both swimming speed means and track displacement lengths were
197 extracted from the acquired data (Figures 5B, S5, and S6). Figure 5B (left panel) shows that the
198 mean velocity of $NB11_{VSG2}$ treated cells was reduced compared to that of untreated cells, while
199 $NB9_{VSG2}$, $NB14_{VSG2}$ and $NB19_{VSG2}$ treated cells behaved largely like the control. A comparison of
200 the track displacement length per second also showed smaller values with a narrower range of
201 distribution in $NB11_{VSG2}$ treated cells (Figure 5B, right panel).

202 As productive movement of trypanosomes was hampered under the influence of $NB11_{VSG2}$
203 (1.7-fold molar excess), the viability of these cells was analyzed in hourly intervals for 8 hours
204 via flow cytometry (Figures 5C and S7). One hour after $NB11_{VSG2}$ addition at least 80 % of treated
205 cells were still alive, with the proportion of dead cells increasing continuously up to 8 hours when
206 about 25 % of cells were still alive (Figure 5C and Table S3). The amount of nanobody used had
207 a critical impact on cell death (Figure S8, Table S3). A 1:1 molar ratio of $NB11_{VSG2}$ to VSG2
208 monomer was required and sufficient to induce cell death within 5 h of induction (consistent with
209 previous reports (Caljon et al., 2012)) with a sharp rise in the number of dead cells observed
210 between samples with a 0.9- and 1.1-fold excess, whilst higher Nb concentrations did not alter the
211 kinetics of the cellular response, suggesting that the VSG coat had been saturated with nanobody
212 (Figure S8B). Based on these results all further experiments were carried out with a saturating 1.7-
213 fold excess of nanobody to VSG monomer.

214 We first explored whether nanobody binding might affect VSG diffusion in the cell surface
215 coat. Fluorescence recovery after photobleaching (FRAP) experiments were performed on

216 immobilized cells whose surface proteins had been fluorescently labeled. VSGs of untreated cells
217 exhibited a median mobile fraction of 83 % and diffusion coefficient of 0.020 $\mu m^2/s$. Addition of
218 the Nb resulted in a marked reduction of the median mobile fraction to 11 % with the diffusion
219 coefficient reduced to a median of 0.007 $\mu m^2/s$ (Figure 5D, left and right graph, respectively).
220 Hence, binding of $NB11_{VSG2}$ to VSG2 on the cell surface significantly affected the mobility of the
221 protein in the cell surface coat.

222 As depicted in Figure 5A, a severe restriction in motility was observed in ensemble
223 measurements between 5 and 15 min after addition of $NB11_{VSG2}$. This time period was therefore
224 chosen to acquire high-speed videos of treated and untreated individual cells (Figures 5E and F,
225 Videos S1 and S2). Nanobody-treated parasites were unable to swim productively. The flagellar
226 wave initiated at the tip of the flagellum, but did not progress through the whole cell body so that
227 the typical cellular waveform could not be observed (Bargul et al., 2016). The parasites were partly
228 paralyzed with increased stiffness and decreased ability to bend the cell body. This observation led
229 us to inspect the nanobody treated cells by electron microscopy.

230

231 **$NB11_{VSG2}$ Induces the Formation of Nanovesicles and Nanotubes on the Trypanosome**
232 **Surface**

233 Interestingly, scanning electron microscopy (SEM) of $NB11_{VSG2}$ treated VSG2-expressing
234 cells revealed the formation of nanovesicles and nanotube-like structures as early as 2 minutes
235 following addition of the nanobody (Figure 6, A and B). Initially, nanovesicles of around 200 nm
236 diameter originated mainly from the flagellum attachment zone (FAZ), the flagellar tip (FT) and
237 the posterior pole (PP) of the cell (Figure 6, A and B; Figure S9A, middle and lower inset). In
238 some parasites, the nanovesicles had formed vesicle chains (Figure 6B). In addition to these

239 nanovesicles and vesicle chains, nanotubes of slightly smaller diameter, that could be more than
240 1 µm in length appeared perpendicular to the FAZ (Figure S9A, upper inset). In the vast majority
241 of cells, nanovesicles and/or nanotubes had been formed after 2 min, while after 5 min all parasites
242 revealed this phenotype. Vesicles appeared on both sides of the FAZ and frequently at the origin
243 of the flagellum, the flagellar pocket (FP) (Figure S9, B and C). Likewise, nanotubes were present
244 in the vicinity of the FP (Figure S9C, left inset). Vesicles in close proximity to the FP tended to be
245 larger (275 nm) than those appearing at the FAZ (150 - 180 nm). In some trypanosomes, the
246 nanovesicles appearing alongside the FAZ seemed to fuse (Figure S9C, right inset), or to
247 redistribute towards the flagellar membrane. However, after 10 min of nanobody incubation,
248 nanovesicles and nanotubes were still present with roughly the same abundance, and, with very
249 little indication of a transition of nanovesicular chains to nanotubes suggesting that both structures
250 form independently (Figure 6C). After 15 min, the number of budding nanovesicles had decreased,
251 and the nanotubes were greatly elongated, thereby apparently forming bridges between parasites.
252 Some of the tubes seemed to be under tension (Figure S9D), while others formed catenated
253 structures.

254 Occasionally, smaller nanotubes or nanovesicles appeared to branch off the main tube (Figure
255 S9D, lower inset). The fact that most of the tens of micrometer long tubes were intact, without
256 showing breakpoints suggests that they are mechanically rather robust. This can be seen when
257 tubes bend around trypanosomes (Figure S9D, middle inset). These rigid membrane ropes may
258 well have additionally hampered trypanosome motility, as the parasites can be literally trapped in
259 a nanotubular network. A closer inspection of the apparent network built from nanotubes revealed
260 that most intersections in fact are crossings of two tubes without fusion (Figure S10A, upper inset),
261 while other intersections seemed to represent true membrane fusion (Figure S10A, lower inset).

262 The presence in nanotubes of nodes of similar size as nanovesicles is first seen after 20 minutes
263 (Figure S10A, middle inset). The endpoint of our observation window was 25 minutes, when the
264 nanotubes had formed concatenated or branched networks that are very difficult to trace by SEM
265 (Figure S10B). However, it seems noteworthy that at this time point nanovesicles also emanated
266 from the same trypanosome membrane areas as after 2 minutes of nanobody incubation, namely
267 along the FAZ, at the posterior pole and at the flagellar tip (Figure S10B). Interestingly, when we
268 looked at control parasites that had undergone the same experimental procedure, but without
269 exposure to the nanobody, we occasionally also observed nanovesicle formation at the FAZ, the
270 FT and the FP. Despite most trypanosomes displaying no or few nanovesicles (Figure S10C,
271 25 min), short nanovesicular chains could be observed in some parasites (Figure S10C, 10 min).
272 This suggests that the formation of nanovesicles at distinct cell surface subcompartments is a
273 biologically relevant process that can be triggered in a spectacular manner by anti-VSG nanobodies
274 (Figure S11).

275

276 **Nanovesicles and Nanotubes are Coated with VSGs and Bud from the Cell Surface**

277 To obtain more detailed information about the ultrastructure of the nanovesicles and
278 nanotubes, ultra-thin sections of trypanosomes, treated with nanobody for 15 min, were prepared
279 for transmission electron microscopy (TEM). The micrographs revealed an intracellular
280 architecture that was indistinguishable from that found in non-treated parasites. Figure S12A
281 shows perfect preservation of flagellar pocket structure, including the tight junction at the flagellar
282 pocket collar, the flagellar pocket matrix and the VSG coat. Frequently, clathrin coated pits were
283 visible, indicating that the endocytosis machinery was at least structurally not impaired. Circular
284 and flat endosomal cisternae were present, as well as class 2 clathrin coated vesicles (CCV II),

285 which are essential for cargo transport to late endosomes (Figure 6D) (Grünfelder et al., 2003).
286 Likewise, mitochondrion, nucleus, endoplasmic reticulum, acidocalcisomes, glycosomes, Golgi
287 and the subpellicular microtubule corset did not show any significant alterations (Figures 6E and
288 S12B). Hence, 15 min post-incubation with nanobodies, the parasite's intracellular architecture
289 was not impaired. Nevertheless, just as in SEM preparations, nanovesicles and nanotubes were
290 readily observable in these TEM samples. These vesicles were covered with an electron-dense
291 layer characteristic of the trypanosome's VSG surface coat, which was confirmed by
292 immunofluorescence analysis (Figure S13).

293 Interestingly, nanovesicles were found to be budding into the flagellar pocket. Figure 6D
294 shows a perfectly spherical budding vesicle, that is decorated with evenly spaced structures. The
295 inner diameter of this vesicle is 100 nm, and the outer structures have a size of about 20 nm, which
296 is similar to the size of membrane-embedded VSGs. Note that a clathrin-coated pit is being formed
297 at the same flagellar pocket. Interestingly, the same cell is shedding nanotubes at the flagellar
298 attachment zone. These are smaller in diameter than the FP-derived nanovesicles. From the
299 micrographs, it is not clear how the nanovesicles exit the FP, as the tight junction and flagellar
300 pocket collar are intact (Figure S12B). Figure 6E shows another example of concomitant formation
301 of large nanovesicles within the flagellar pocket and nanovesicles/nanotubes at the flagellar
302 attachment zone. These structures were probably the nanovesicular chains observed in SEM.
303 Interestingly, the TEM images show that the "vesicles" were not always fully separated by
304 membrane but had continuous content (Figure 6E, lower inset). In all these vesicles, electron-dense
305 particles were detected, which were identical with the cytoplasmic ribosomes in size and form
306 (Figure 6E, lower inset). As the flagellum is free of ribosomes, the segmented nanotubes and free
307 nanovesicles likely originate from the pellicular plasma membrane and not from the flagellum

308 (Figure S12D). In contrast, the smooth and long nanotubes observed with SEM after 15 minutes
309 of treatment, could well originate from the flagellar membrane, as shown in Figure S12C. In this
310 cell, multiple tubes bud from one flagellum. These are also covered by a VSG-coat, but do not
311 contain ribosome-like structures. The shedding of the smooth nanotubes must involve significant
312 mechanical forces, as is suggested by marked membrane deformations, both on the flagellar side
313 and on the nanotubes (Figure S12C, white arrows). In rare occasions, a nanotube branchpoint was
314 observed (Figure S12E), but it remains unclear how these branches can form. Figure S12F shows
315 that the tubes can be bent and deformed, which is in agreement with observations made in SEM
316 micrographs.

317 In conclusion, we have established that nanobodies can bind deep within the VSG-coat and
318 that binding can rapidly affect VSG mobility within the plasma membrane. Interestingly,
319 nanobody-binding leads to an almost instantaneous formation of nanovesicles and nanotubes on
320 the parasite cell surface, concomitant with stiffening of the cells and loss of parasite motility. Cell
321 death occurs significantly later and is probably a consequence of stalled motion, which inevitably
322 will affect cytokinesis.

323

324 **Discussion**

325

326 Using the camelid immune system to generate a collection of anti-VSG2 nanobodies, we have
327 been able to show through structural, biochemical, and cell biological experiments that nanobodies
328 can bind deeply into the trypanosome surface coat, even to the bottom of the NTD of the VSGs.
329 Using secondary IgG antibodies to detect the nanobodies, we also demonstrate that antibodies of
330 the mammalian immune system are able to reach into the densely packed coat of *T. brucei* to a
331 depth of ~50 Å, but have difficulty reaching further than ~80 Å below the coat surface (Figure

332 7A). Furthermore, using full camelid antibodies with the same nanobody domain, we show that
333 the camelid immune system can reach as far as the nanobodies themselves to bind to epitopes
334 buried as deep as 50 Å.

335 Our experimental results demonstrate that the antigenic surface of the VSGs extends well
336 beyond the upper surfaces of these molecules. Such conclusions are consistent with the
337 observations that the VSGs possess molecular surfaces with relatively high sequence divergence
338 as well as markedly distinguishing surface properties not only at the "top" of the NTD, but across
339 the entire molecule (Figure 7B). That the much more highly conserved CTD would be difficult for
340 antibodies to access (located more than 100 Å below the surface) as shown previously (Schwede
341 et al., 2011) and in our study, is also in harmony with this model.

342 We identified one Nb ($NB11_{VSG2}$) that was highly efficient in immobilizing and ultimately
343 killing cells, a marked motility phenotype which is in accordance with published work (Stijlemans
344 et al., 2011). In contrast, our work does not support the conclusion that this is due to impaired
345 endocytosis and hence impaired energy supply. The onset of the motility phenotype was within
346 minutes of nanobody addition and electron micrographs did not reveal any disruption in the
347 endomembrane system, including the endosomes. What we observed was a marked reduction in
348 cell body flexibility and increased stiffness of parts of the cell. This was not caused by paralysis
349 of the flagellum as it still initiated the beat which was however not propagated over the cell body.
350 Hence, the trypanosomes did not swim anymore. We hypothesize that the phenotype observed
351 could be related to the mobility and integrity of the surface coat. We have previously shown that
352 the VSG coat operates very close to a molecular crowding threshold, where a high lateral mobility
353 is balanced with the highest possible density of the protein (Hartel et al., 2016). When the VSG
354 density exceeds this threshold, translational diffusion in the surface coat is severely affected. This

355 is exactly what might occur in the experiments reported here. Binding of the nanobody increases
356 the hydrodynamic radius of the VSG dimers which results in a dramatic decrease in the mobile
357 fraction. Thus, rotational and translational diffusion of the VSGs is confined by steric hindrance.
358 Thermodynamics in confinement would cause tension within the VSG coat due to pressure forces.
359 If this were the case, there should be ultrastructural changes in surface topology of the
360 trypanosomes. Indeed, we observed dramatic changes of the trypanosome cell surface in electron
361 micrographs.

362 Membrane fission is essential for the life of all cells. Cytokinesis, the generation of organelles
363 such as the mitochondrion, ER and Golgi, as well as endomembrane trafficking are processes that
364 all depend on this type of membrane remodeling. Complex machineries involving many proteins
365 that can form helical scaffolds or constricting rings, as well as shallow membrane insertions, are
366 thought to control membrane fission (Snead et al., 2017; Campelo and Malhotra, 2012). Classic
367 examples are the clathrin or COP pathways and the ESCRT machinery. These pathways are well-
368 controlled in space and time, and they are highly energy-consuming. The total energy of membrane
369 vesiculation has been estimated to be in the range of several hundred k_BT, which means that
370 membrane fission requires significant mechanical forces, acting from outside onto the membrane.
371 This is exemplified by the massive clathrin assembly visible on a coated pit at the flagellar pocket
372 in Figure S12A.

373 The nanovesicles and nanotubes observed in this work on the trypanosome cell surface did
374 not show any structural features that differed from the plasma membrane. They were decorated
375 with an electron dense VSG layer but no additional coats that could be involved in vesicle
376 formation were detectable. This is not unexpected, as it is very unlikely that the parasites can sense
377 the nanobody addition, transduce this information and actively secrete a putative extracellular

378 fission-promoting machinery - all within seconds. Thus, it is most probably not an active cellular
379 process that drives nanovesicle and nanotube formation.

380 An attractive, alternative explanation for the phenotype would be protein-protein crowding.
381 The addition of nanobodies to the extremely dense VSG coat could - within seconds - raise the
382 protein density on the cell surface above the molecular crowding threshold. In fact, we have shown
383 that the lateral mobility of the VSG decreases rapidly after nanobody addition, which supports this
384 assumption. With the binding of nanobodies, mobility of the VSG becomes restricted and the coat
385 is therefore under tension. Collisions of nanobody-loaded VSGs will generate pressure (on one
386 side of the plasma membrane). This behavior of a crowded membrane protein has been likened to
387 that of compressed gas and it has been suggested to provide the pressure force required to initiate
388 and complete membrane vesiculation and tubulation (Snead et al., 2017). Thus, nanobody-
389 mediated protein crowding could provide the energy required for membrane fission. No cellular
390 machineries would be required to overcome the energy barrier. Membrane fission by protein-
391 protein crowding has been observed before, albeit only in artificial systems and is supported by
392 modeling approaches (Derganc and Čopič, 2016; Snead et al., 2017).

393 Our data suggest that this mechanism could also function in the cellular context. Due to its
394 uniformity, the trypanosome coat with its high density and essential mobility of the VSG is an
395 ideal model system to study this new mechanism of membrane fission in living cells. The fact that
396 we find nanotubes and nanovesicles also in untreated cells, albeit only occasionally, suggests that,
397 at least in trypanosomes, protein crowding-mediated extracellular vesiculation could be a
398 biologically relevant process. We surmise that by using this passive, density-controlled process,
399 the parasites can adjust the VSG-coat density, e.g. during cell division or VSG switching. Protein

400 crowding-mediated membrane shedding may well be effective on other cells with dense protein
401 coats.

402 Especially at early time points after addition of nanobodies, vesicle chains of increasing length
403 were observed. TEM images showed that the chains were not always composed of separated
404 vesicles but were often segmented, continuous volumes. There are few reports on vesicle chains
405 in biology. Outer membrane vesicle chains have been reported in *Myxococcus xanthus* (Remis et
406 al., 2014) and biopearling has been observed in a marine flavobacterium (Fischer et al., 2019).
407 However, the mechanisms underlying vesicle chain formation have not been studied. As
408 segmented membrane volumes are detectable already after 2 minutes in nanobody-treated
409 trypanosomes, we surmise that counteracting mechanical forces interrupt full fission of
410 nanovesicles. The segmented vesicle chains mainly appear at the FAZ and the flagellar pocket.
411 These regions continuously experience the forces exerted by the flagellar beat. It is tempting to
412 speculate that the flagellar force causes interruption of fission events. The protein crowding
413 pressure on the nascent vesicle could be strong enough to maintain the vesicle curvature. When a
414 new vesicle forms at the same position of the FAZ it would be connected to the previous one. In
415 this way, the continuous beat of the flagellum would produce segments of very similar size. After
416 about 15 minutes of nanobody treatment, the vesicle chains disappear. This is the time point when
417 the propagation of the flagellar beat is impaired, probably due to membrane tension caused by loss
418 of membrane through vesiculation. Thus, the force producing the segmented membrane volumes
419 decreases, resulting in a shift to tubulation. The resulting nanotubes can be tens of micrometers
420 long, and the wiggling cells entangle themselves in these rope-like structures. It is important to
421 note that fusion of nanotubes to neighboring parasites has not been observed, suggesting that cell-
422 cell communication via membrane bridges is not occurring.

423 In summary, the fast onset of membrane fission at "free" membrane compartments could be
424 explained by membrane tubulation through protein-protein crowding on the trypanosome cell
425 surface. Are the nanovesicles in fact exosomes or ectosomes (extracellular vesicles, EVs)?
426 Exosomes are produced by multivesicular bodies and secreted by exocytosis. This has previously
427 been observed in fly-stage *T. brucei* procyclic forms (Eliaz et al., 2017). Since we did not find any
428 changes in the endomembrane architecture, the vesicles formed after nanobody treatment are likely
429 not exosomes. The formation of extracellular vesicles in trypanosomes was first reported in 2016
430 (Szempruch et al., 2016). In contrast to our data, this work revealed that EVs were generated by
431 vesiculation of nanotubes that are highly fusogenic and originate from the flagellar membrane.
432 Thus, despite morphological similarities, the nanovesicles and nanotubes observed in the present
433 study are neither exosomes nor ectosomes, but rather the product of membrane fission through
434 protein-protein crowding. The trypanosome-nanobody system for the first time enables us to
435 systematically study a highly efficient mechanism by which the crowded protein environment on
436 the surface of cells causes changes in membrane shape.
437
438

439 **REFERENCES**

440 Arbabi-Ghahroudi, M. (2017). Camelid Single-Domain Antibodies: Historical Perspective and
441 Future Outlook. Front Immunol *8*.

442 Bangs, J.D. (2018). Evolution of Antigenic Variation in African Trypanosomes: Variant Surface
443 Glycoprotein Expression, Structure, and Function. BioEssays *40*, 1800181.

444 Bargul, J.L., Jung, J., McOdimba, F.A., Omogo, C.O., Adung'a, V.O., Kruger, T., Masiga, D.K.,
445 and Engstler, M. (2016). Species-Specific Adaptations of Trypanosome Morphology and
446 Motility to the Mammalian Host. PLoS Pathog *12*, e1005448.

447 Bartossek, T., Jones, N.G., Schafer, C., Cvitkovic, M., Glogger, M., Mott, H.R., Kuper, J.,
448 Brennich, M., Carrington, M., Smith, A.S., et al. (2017). Structural basis for the shielding
449 function of the dynamic trypanosome variant surface glycoprotein coat. Nat Microbiol *2*, 1523–
450 1532.

451 de Beer, T.A.P., Berka, K., Thornton, J.M., and Laskowski, R.A. (2014). PDBsum additions.
452 Nucleic Acids Res *42*, D292–D296.

453 Borst, P. (2002). Antigenic variation and allelic exclusion. Cell *109*, 5–8.

454 Bülow, R., Overath, P., and Davoust, J. (1988). Rapid lateral diffusion of the variant surface
455 glycoprotein in the coat of Trypanosoma brucei. Biochemistry *27*, 2384–2388.

456 Caljon, G., Stijlemans, B., Saerens, D., Abbeele, J.V.D., Muyldermans, S., Magez, S., and
457 Baetselier, P.D. (2012). Affinity Is an Important Determinant of the Anti-Trypanosome Activity
458 of Nanobodies. PLOS Neglected Tropical Diseases *6*, e1902.

459 Campelo, F., and Malhotra, V. (2012). Membrane Fission: The Biogenesis of Transport Carriers.
460 Annu. Rev. Biochem. *81*, 407–427.

461 Derganc, J., and Čopič, A. (2016). Membrane bending by protein crowding is affected by protein
462 lateral confinement. Biochim. Biophys. Acta *1858*, 1152–1159.

463 Eliaz, D., Kannan, S., Shaked, H., Arvatz, G., Tkacz, I.D., Binder, L., Waldman Ben-Asher, H.,
464 Okalang, U., Chikne, V., Cohen-Chalamish, S., et al. (2017). Exosome secretion affects social
465 motility in Trypanosoma brucei. PLoS Pathog *13*, e1006245.

466 Engstler, M., Thilo, L., Weise, F., Grunfelder, C.G., Schwarz, H., Boshart, M., and Overath, P.
467 (2004). Kinetics of endocytosis and recycling of the GPI-anchored variant surface glycoprotein
468 in Trypanosoma brucei. J Cell Sci *117*, 1105–1115.

469 Engstler, M., Pfohl, T., Herminghaus, S., Boshart, M., Wiegertjes, G., Heddergott, N., and
470 Overath, P. (2007). Hydrodynamic flow-mediated protein sorting on the cell surface of
471 trypanosomes. Cell *131*, 505–515.

472 Fischer, T., Schorb, M., Reintjes, G., Kolovou, A., Santarella-Mellwig, R., Markert, S., Rhiel, E.,
473 Littmann, S., Becher, D., Schweder, T., et al. (2019). Biopearling of Interconnected Outer
474 Membrane Vesicle Chains by a Marine Flavobacterium. App. Environ. Microbiol. *85*.

475 Grünfelder, C.G., Engstler, M., Weise, F., Schwarz, H., Stierhof, Y.-D., Morgan, G.W., Field,
476 M.C., and Overath, P. (2003). Endocytosis of a glycosylphosphatidylinositol-anchored protein
477 via clathrin-coated vesicles, sorting by default in endosomes, and exocytosis via RAB11-positive
478 carriers. Mol. Biol. Cell *14*, 2029–2040.

479 Hartel, A.J., Glogger, M., Jones, N.G., Abuillan, W., Batram, C., Hermann, A., Fenz, S.F.,
480 Tanaka, M., and Engstler, M. (2016). N-glycosylation enables high lateral mobility of GPI-
481 anchored proteins at a molecular crowding threshold. Nat Commun *7*, 12870.

482 Hartel, A.J.W., Glogger, M., Guigas, G., Jones, N.G., Fenz, S.F., Weiss, M., and Engstler, M.
483 (2015). The molecular size of the extra-membrane domain influences the diffusion of the GPI-
484 anchored VSG on the trypanosome plasma membrane. Scientific Reports *5*, 10394.

485 Horn, D. (2014). Antigenic variation in African trypanosomes. Mol Biochem Parasitol *195*, 123–
486 129.

487 de Marco, A. (2011). Biotechnological applications of recombinant single-domain antibody
488 fragments. Microb Cell Fact *10*, 44.

489 McNicholas, S., Potterton, E., Wilson, K.S., and Noble, M.E.M. (2011). Presenting your
490 structures: the CCP4mg molecular-graphics software. Acta Crystallogr D Biol Crystallogr *67*,
491 386–394.

492 Mugnier, M.R., Stebbins, C.E., and Papavasiliou, F.N. (2016). Masters of Disguise: Antigenic
493 Variation and the VSG Coat in Trypanosoma brucei. PLoS Pathog *12*, e1005784.

494 Overath, P., Chaudhri, M., Steverding, D., and Ziegelbauer, K. (1994). Invariant surface proteins
495 in bloodstream forms of Trypanosoma brucei. Parasitology Today *10*, 53–58.

496 Pal, A., Hall, B.S., Jeffries, T.R., and Field, M.C. (2003). Rab5 and Rab11 mediate transferrin
497 and anti-variant surface glycoprotein antibody recycling in Trypanosoma brucei. Biochem J *374*,
498 443–451.

499 Pettersen, E.F., Goddard, T.D., Huang, C.C., Couch, G.S., Greenblatt, D.M., Meng, E.C., and
500 Ferrin, T.E. (2004). UCSF Chimera--a visualization system for exploratory research and
501 analysis. J Comput Chem *25*, 1605–1612.

502 Radwanska, M., Vereecke, N., Deleeuw, V., Pinto, J., and Magez, S. (2018). Salivarian
503 Trypanosomosis: A Review of Parasites Involved, Their Global Distribution and Their
504 Interaction With the Innate and Adaptive Mammalian Host Immune System. Front. Immunol. *9*,
505 2253.

506 Remis, J.P., Wei, D., Gorur, A., Zemla, M., Haraga, J., Allen, S., Witkowska, H.E., Costerton,
507 J.W., Berleman, J.E., and Auer, M. (2014). Bacterial social networks: structure and composition
508 of Myxococcus xanthus outer membrane vesicle chains. Environ. Microbiol. *16*.

509 Schwede, A., Jones, N., Engstler, M., and Carrington, M. (2011). The VSG C-terminal domain is
510 inaccessible to antibodies on live trypanosomes. Mol Biochem Parasitol *175*, 201–204.

511 Schwede, A., Macleod, O.J., MacGregor, P., and Carrington, M. (2015). How Does the VSG
512 Coat of Bloodstream Form African Trypanosomes Interact with External Proteins? PLoS Pathog
513 *11*, e1005259.

514 Snead, W.T., Hayden, C.C., Gadok, A.K., Zhao, C., Lafer, E.M., Rangamani, P., and
515 Stachowiak, J.C. (2017). Membrane fission by protein crowding. Proc. Natl. Acad. Sci. USA
516 *114*, E3258–E3267.

517 Stijlemans, B., Conrath, K., Cortez-Retamozo, V., Van Xong, H., Wyns, L., Senter, P., Revets,
518 H., De Baetselier, P., Muyldermans, S., and Magez, S. (2004). Efficient targeting of conserved
519 cryptic epitopes of infectious agents by single domain antibodies. African trypanosomes as
520 paradigm. J. Biol. Chem. *279*, 1256–1261.

521 Stijlemans, B., Caljon, G., Natesan, S.K.A., Saerens, D., Conrath, K., Pérez-Morga, D., Skepper,
522 J.N., Nikolaou, A., Brys, L., Pays, E., et al. (2011). High Affinity Nanobodies against the
523 Trypanosome brucei VSG Are Potent Trypanolytic Agents that Block Endocytosis. PLoS Pathog
524 *7*.

525 Stijlemans, B., De Baetselier, P., Caljon, G., Van Den Abbeele, J., Van Ginderachter, J.A., and
526 Magez, S. (2017). Nanobodies As Tools to Understand, Diagnose, and Treat African
527 Trypanosomiasis. Front Immunol *8*.

528 Szempruch, A.J., Sykes, S.E., Kieft, R., Dennison, L., Becker, A.C., Gartrell, A., Martin, W.J.,
529 Nakayasu, E.S., Almeida, I.C., Hajduk, S.L., et al. (2016). Extracellular Vesicles from
530 Trypanosoma brucei Mediate Virulence Factor Transfer and Cause Host Anemia. Cell *164*, 246–
531 257.

532 Webster, P., Russo, D.C., and Black, S.J. (1990). The interaction of Trypanosoma brucei with
533 antibodies to variant surface glycoproteins. J Cell Sci *96 (Pt 2)*, 249–255.

534
535

536 **SUPPLEMENTARY FIGURES AND TABLES**

537 Figures 1-15, Table 1-3

538 **ACKNOWLEDGEMENTS**

539 We acknowledge synchrotron time at the Diamond Light Source (DLS, beamline i03, Neil
540 Paterson and colleagues and the Paul Scherrer Institut, Villingen, Switzerland (SLS, beamline
541 PXIII, Vincent Olieric and colleagues). We thank Steve Schoonooghe, Ema Estevens Romão, and
542 Gholamreza Hassanzadeh Ghassabeh of the Vlaams Instituut voor Biotechnologie (VIB)
543 Nanobody Core facility for working closely with us to produce anti-VSG2 VHH antibodies and
544 donating for experimental controls the antibody to *H. pylori* BabA. We thank Elisabeth Meyer-
545 Natus (Würzburg) for technical assistance with EM sample preparation and data acquisition. We
546 thank Tim Krüger (Würzburg) for assistance with microscopy and Susanne Fenz (Würzburg) for
547 helpful discussions. M.E. is supported by DFG grants EN305, DFG-SPP1726, DFG-GRK2157
548 and GIF grant I-473-416.13/2018.

549

550 **AUTHOR CONTRIBUTIONS**

551 C.E.S., F.N.P., M.E. and N.G.J. conceived, initiated and coordinated the project, M.vS. produced
552 VSG2 for production of nanobodies. M.vS. and A.H. produced and crystallized $NB11_{VSG2}$ and
553 $NB14_{VSG2}$ complexes. A.H. produced and crystallized $NB9_{VSG2}$ and $NB19_{VSG2}$ complexes, all
554 complexes for membrane studies (with M.vS. also producing $NB11_{VSG2}$ and $NB14_{VSG2}$ for the
555 latter), collected the diffraction data and solved all structures. J.Z. aided in crystal preparation and
556 beamline data collection. H.H. and A.H. created sortaggable Nbs and the camelid heavy chain Ig2.
557 H.H., M.vS, and A.H performed anti-His FACs binding experiments. H.H and A.H produced the

558 FAM and FITC FACS data on live *T. brucei*, while A.H. executed FACS experiments on non-
559 VSG2 coats. L.H. performed all electron microscopy, parasite movement, coat diffusion, and
560 toxicity experiments. C.E.S., A.H., N.G.J. and M.E. wrote the manuscript. All authors discussed
561 the data and approved the final manuscript.

562 **DECLARATION OF INTERESTS**

563 The authors declare that they have no competing interests.

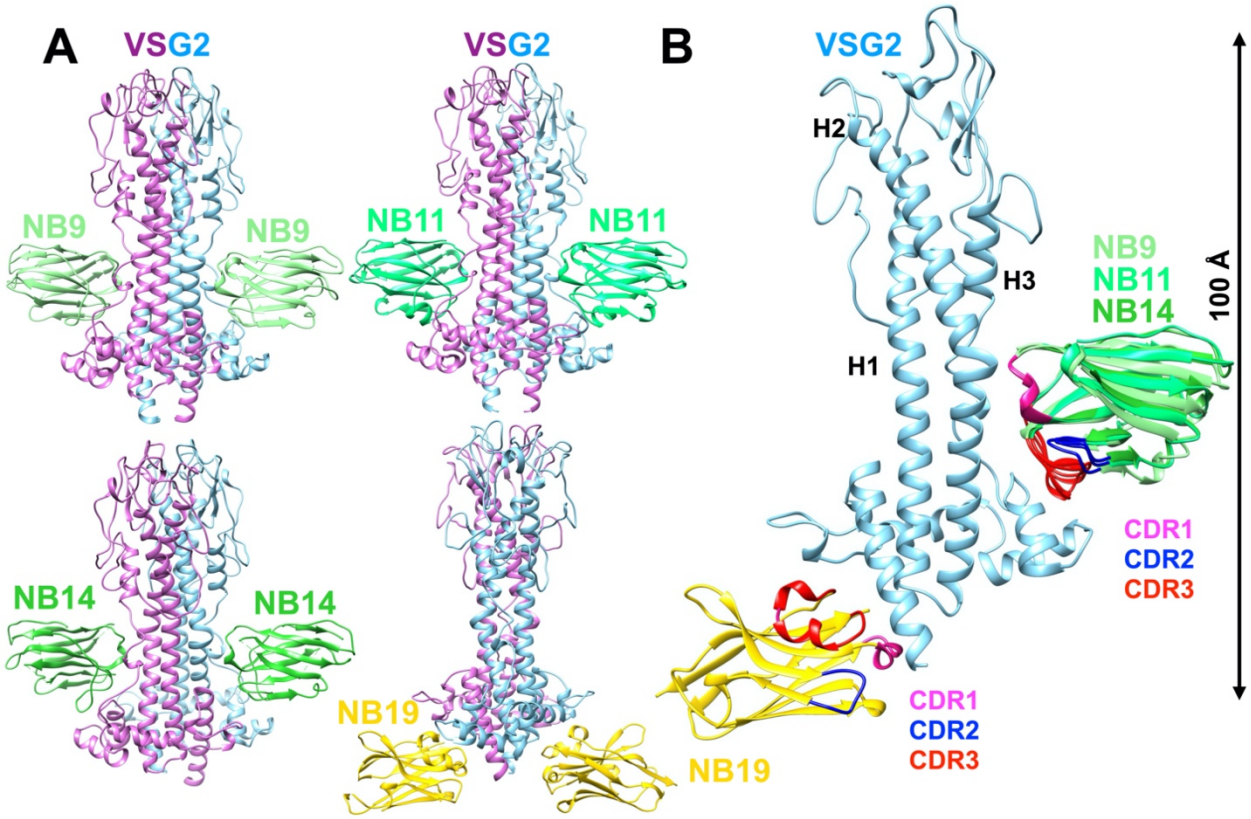

564

565 **Figure 1. Overall Structures of VSG2-NB Complexes**

566 **(A)** The four nanobody-VSG2 structures with $NB9_{VSG2}$ (NB9 in light green, top left), $NB11_{VSG2}$
567 (NB11 in lime green, top right), $NB14_{VSG2}$ (NB14 in green, bottom left) and $NB19_{VSG2}$ (NB19 in
568 gold, bottom right) and VSG2 (dimer shown in cyan/purple) are depicted as ribbon diagrams.
569 **(B)** Superposition of VSG2-NB complexes with similar coloring. The Complementarity-
570 Determining Regions (CDR or variable region) are shown in magenta (CDR1), blue (CDR2) and
571 red (CDR3). Structures illustrated with Chimera (Pettersen et al., 2004).

572

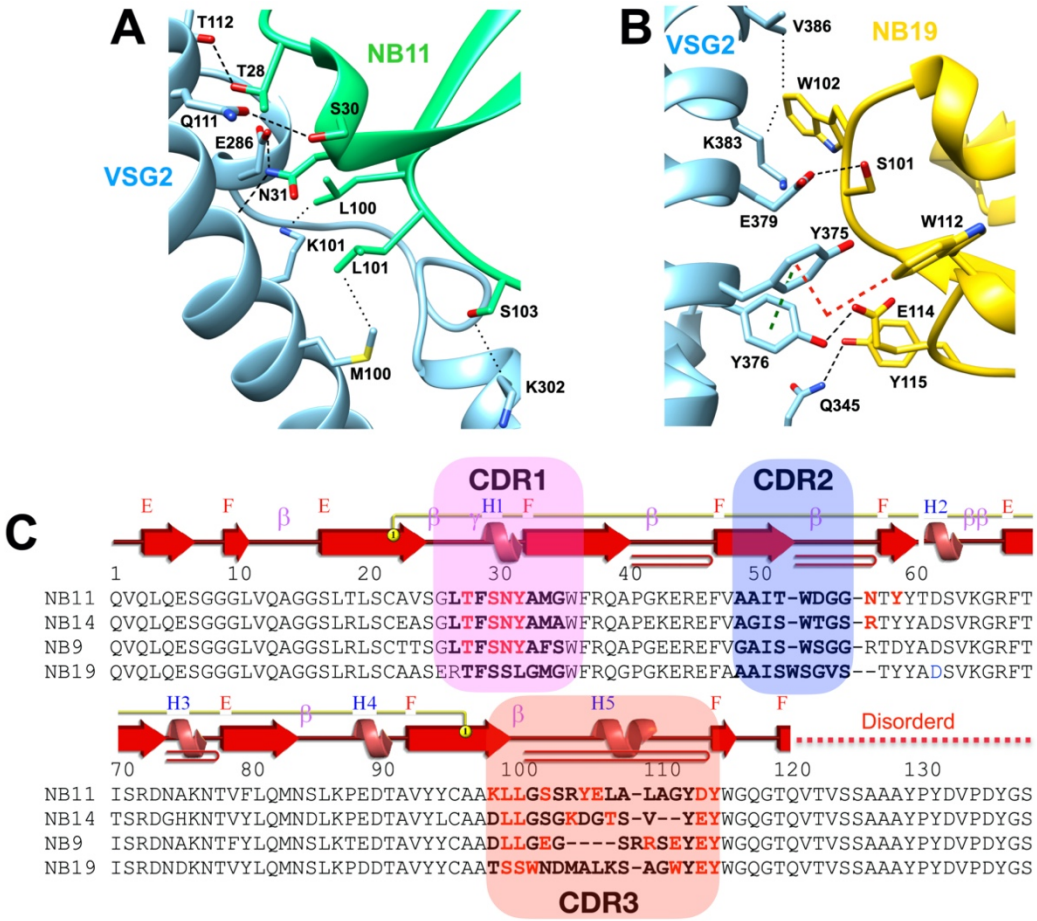

Figure 2. Interactions of Nanobody CDR Variable Loops with VSG2

(A) Close up of the interaction of the CDR3 loop from $NB11_{VSG2}$ (NB11) with VSG2. Side chains from each protein have carbon atoms colored to match the ribbon diagram of the main chain, with atoms of oxygen, nitrogen, and sulfur shown in red, blue, and yellow, respectively. Hydrogen bonds (black bricks) are formed between T28, S30 and N31 (NBs) with T112, Q111 and E286 (VSG2), respectively. Residues L100, L101 and S103 of NB11 were found to form non-covalent (black dots) bonds with K101, M100 and K302 of VSG2. **(B)** Close up of the interaction of the CDR3 loop from NB19 with VSG2. Hydrogen bonds (black bricks) are formed between S101 (NB19) and E379 (VSG2), as well as between Y115 (NB19) and Q345 (VSG2). Residues W102

583 (NB19) and V386 and K383 were involved in non-covalent interactions. W112 of NB19 interacts
584 with Y375 of VSG2 in a parallel displaced π-stacking (red bricks) manner. This interaction is
585 further reinforced by a VSG2 intra-molecule T-shaped π-stacking (green bricks) between Y375
586 and Y376. **(C)** Sequence alignment and annotation of the four Nbs (numbering is for $NB11_{VSG2}$),
587 including secondary structural elements is shown together with highlighted regions of the CDR
588 variable loops (colored as in Figure 1b). Residues that make contacts with VSG2 are shown with
589 red letters. Structures illustrated with Chimera (Pettersen et al., 2004) and secondary structure with
590 PDBSum (de Beer et al., 2014).

591

592

593

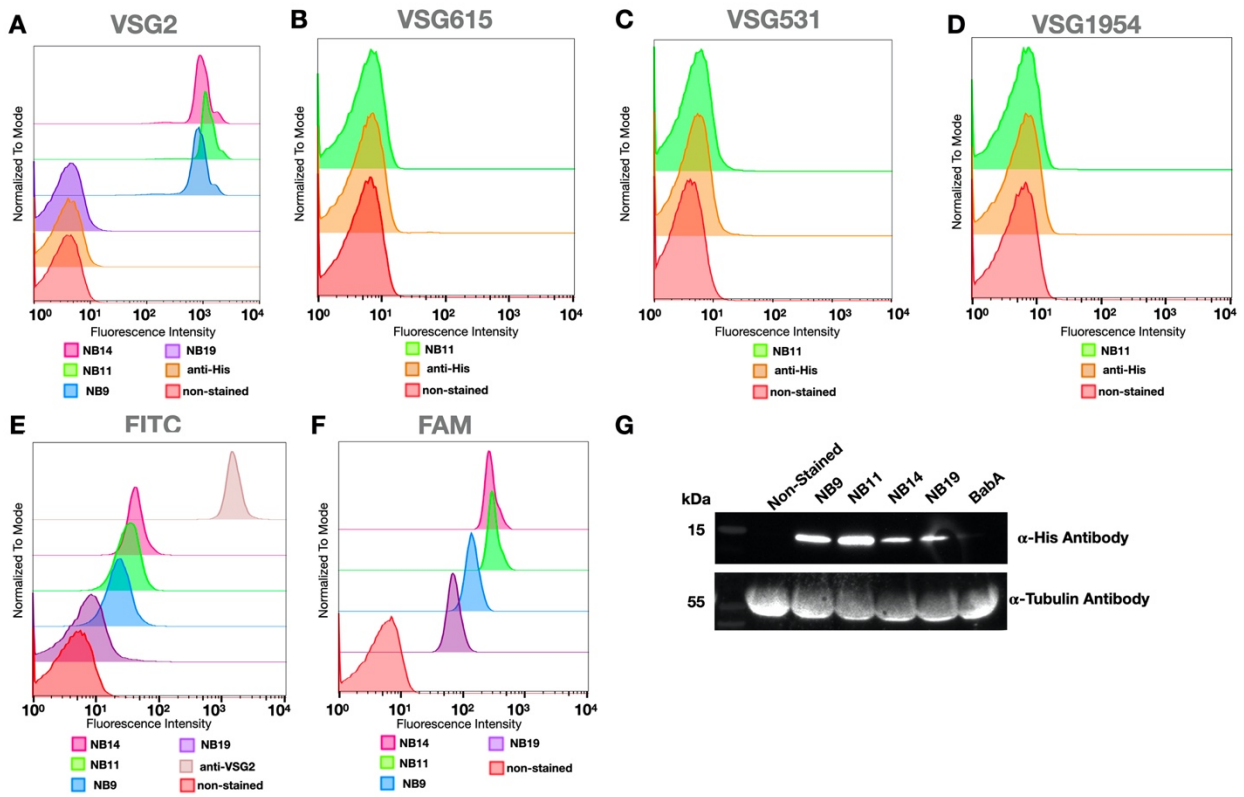

594

595 **Figure 3. Binding Assays of Nbs to Live Trypanosomes** Different VSG-expressing *T. brucei*
596 were incubated with various Nbs and visualized in different ways by FACS. **(A)** VSG2-
597 expressing bloodstream form (BSF) trypanosomes were incubated with C-terminally His-tagged
598 Nbs and visualized using an anti-His antibody, **(B)** VSG615-expressing BSF trypanosomes
599 (expressing a metacyclic VSG) were incubated with C-terminally His-tagged Nbs and visualized
600 using an anti-His antibody, **(C)** VSG531-expressing BSF trypanosomes were incubated with C-
601 terminally His-tagged Nbs and visualized using an anti-His antibody, **(D)** VSG1954-expressing
602 BSF trypanosomes (expressing a metacyclic VSG) were incubated with C-terminally His-tagged
603 Nbs and visualized using an anti-His antibody, **(E)** VSG2-expressing bloodstream form (BSF)
604 trypanosomes were incubated with FITC-labeled Nbs and visualized through the fluorochrome's

605 emission, **(F)** VSG2-expressing bloodstream form (BSF) trypanosomes were incubated with Nbs
606 sortagged with FAM and visualized through the fluorochrome's emission **(G)** VSG2-expressing
607 bloodstream form (BSF) trypanosomes were incubated with C-terminally His-tagged Nbs,
608 washed thoroughly, run on an SDS-PAGE gel, and probed with an anti-His antibody. An
609 irrelevant Nb (BabA, raised to a protein from *H. pylori*) was used as a negative control. The
610 same cells were probed with an anti-tubulin antibody to provide a gel-loading standard.
611
612

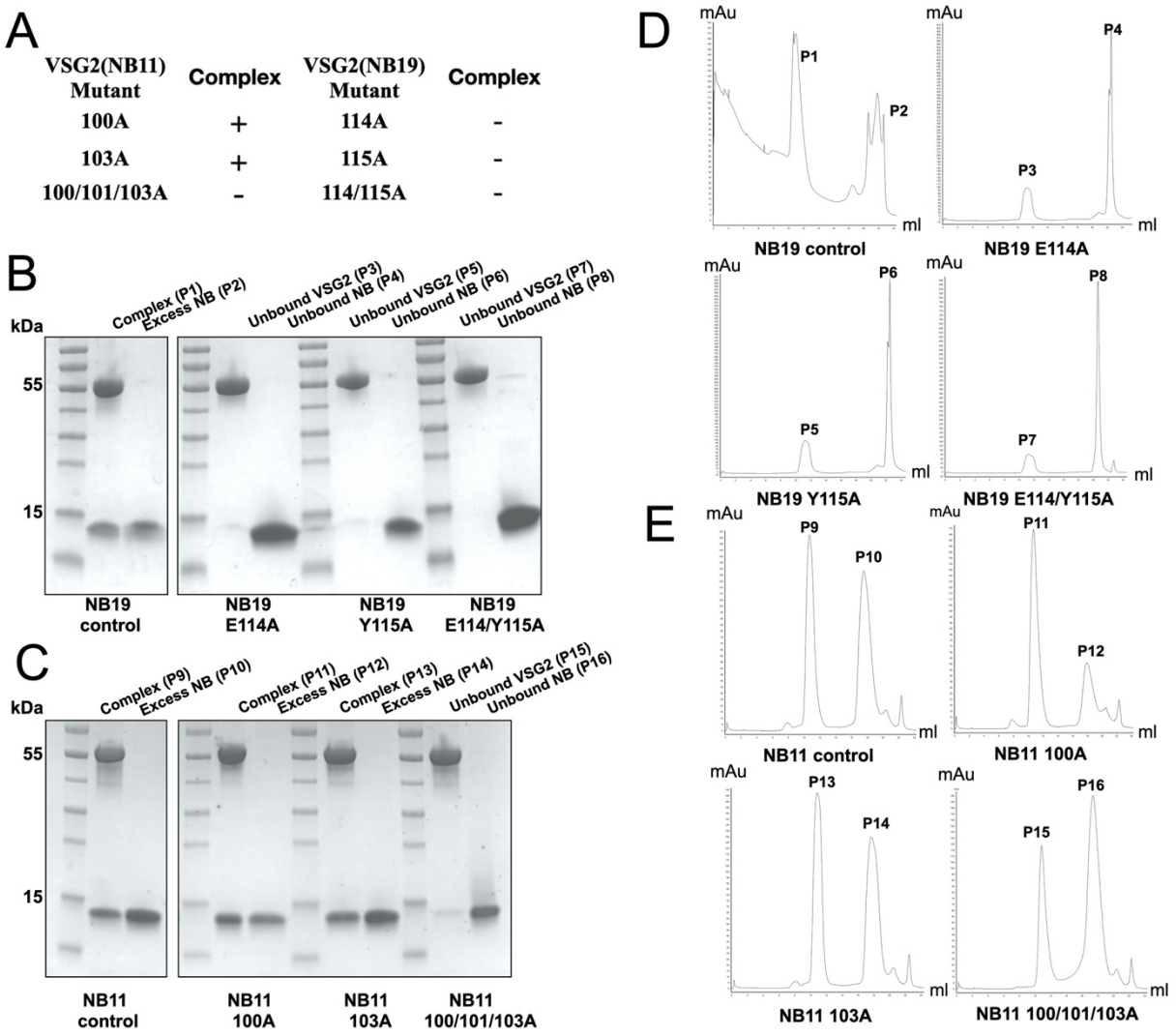

Figure 4. Mutations in the V-Loop Regions of Nanobodies Inhibit Complex Formation with VSG2 . (A) Overview of $NB11_{VSG2}$ and $NB19_{VSG2}$ mutants in relation to their ability to bind VSG2. $NB11_{VSG2}$ mutants L100A and L103A form a complex with VSG2 (+), while the triple mutant L100/L101/S103 does not bind (-). For $NB19_{VSG2}$ all single and multiple mutants (E114A, Y115A, E114/Y115A) fail to form a complex with VSG2 (-). **(B and C)** SDS-PAGE analysis of purified, mixed VSG2 and nanobodies (wild type and mutant $NB11_{VSG2}$ and $NB19_{VSG2}$) analyzed by gel filtration chromatography (see Methods). Peak elution fractions are shown and numbered. VSG2 corresponds to the 55 kDa band and nanobodies to the 15 kDa band. Gels were stained with

622 Coomassie blue. **(D and E)** FPLC chromatographs corresponding to the SDS-PAGE gels **(B and**
623 **C)** with corresponding peak numbers from the SDS-PAGE gels shown. The Y-axis displays the
624 UV_{280nm} absorbance (arbitrary units) and the X-axis the elution volume from the column (see
625 Methods).
626
627
628

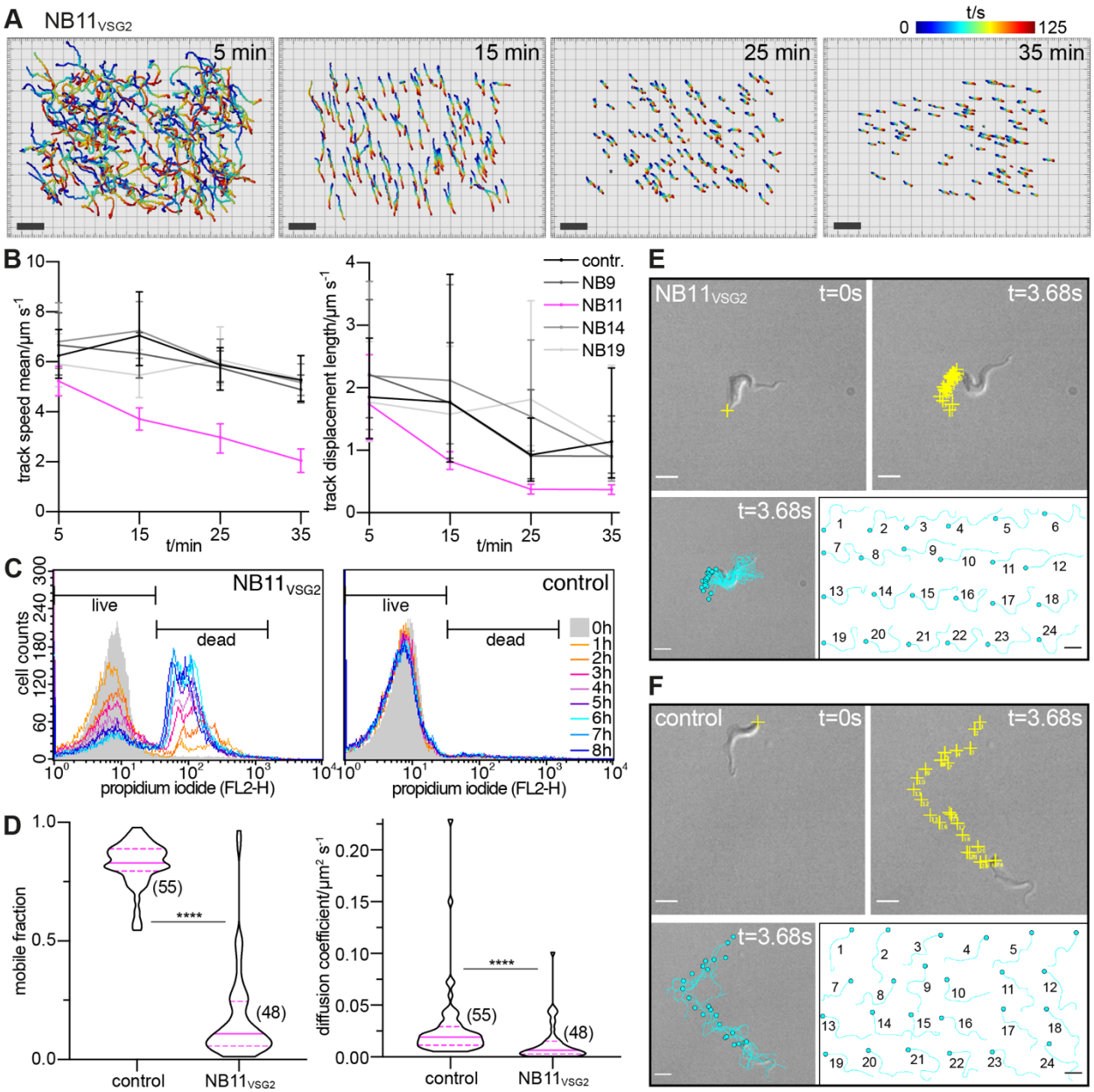

Figure 5. Nanobodies Reduce VSG Mobility, Paralyze, and Kill Trypanosomes **(A-E)** Cells were treated with a 1.7-fold molar excess of Nb to VSG monomer. **(A)** $NB11_{VSG2}$ affects cell motility after 15 min of treatment. Individual cells in a population were tracked for 125 s at 5, 15, 25 and 35 minutes post addition of $NB11_{VSG2}$ and analyzed using the Imaris x64 software. Cells close to the border of the imaging region were removed by filtering to simplify the images shown (s. Figure S4C for trajectories of complete data set). Trajectories are

636 color coded blue (t = 0 s) to red (t = 125 s). Scale bars, 100 µm. **(B)** Comparison of velocities
637 (track speed mean), left, and track displacement lengths per s, right, of untreated cells and cells
638 treated with four different nanobodies, $NB9_{VSG2}$, $NB11_{VSG2}$, $NB14_{VSG2}$ and $NB19_{VSG2}$. Data
639 extracted from trajectories shown in Figure S4 (median with bars representing the 25th and 75th
640 percentile of data points; see Figures S5 and S6 for scatter dot plots of the data). Both velocity and
641 track displacement are clearly most affected upon treatment with $NB11_{VSG2}$.
642 **(C)** Flow cytometry analysis to determine the extent of cell death over time following treatment
643 with $NB11_{VSG2}$. Left panel, treated cells, right panel, untreated control cells analyzed in hourly
644 intervals over a duration of 8 h. Propidium iodide was used as a dead cell marker. Each histogram
645 is based on 25.000 gated events (Figure S7 shows the gate settings for the Nb treated data set).
646 **(D)** The effect of nanobody binding on VSG diffusion was analyzed by fluorescence recovery after
647 photobleaching (FRAP) experiments on immobilized trypanosomes that were surface labeled with
648 ATTO 488. Untreated (control) and $NB11_{VSG2}$ treated cells were analyzed (n in brackets). Violin
649 plots showing the frequency distribution of the mobile fractions, left, and the diffusion coefficient,
650 right, of the VSG in control and $NB11_{VSG2}$ treated cells (median, solid magenta lines; 25th and
651 75th percentile, dashed magenta lines). There was a remarkable reduction in mobile fraction of
652 treated cells, median of 11 %, compared to that of untreated cells, median of 83 %. The median
653 diffusion coefficient of mobile VSGs following treatment with $NB11_{VSG2}$ was reduced to 0.007
654 $\mu m^2/s$ from 0.019 $\mu m^2/s$ for untreated cells. P values from an unpaired, two-tailed Mann-Whitney
655 test (**** = $P<0.001$) are shown in both graphs.

656 **(E, F)** Single cell analysis of an $NB11_{VSG2}$ treated **(E)** and an untreated **(F)** trypanosome. The
657 upper images show the first (left) and last (right) frame of a video (s. Videos S1 and S2) with the
658 posterior of the cell marked by a yellow cross in the first image and the posterior of every 40th
659 frame of the sequence marked in the second image. Whereas the flagellar beat generates a
660 propulsive force in wt cells the Nb treated cells initiate beats without the generation of a propulsive
661 force. Movement is visualized by tracing the cell shape (cyan lengthwise line through the center
662 of the cell with a circle marking the posterior) in every 40th frame, bottom row. Bottom left image,
663 traces at the position of the cell in the video sequence, bottom right images: the same traces
664 displayed individually to show differences in cell shape and orientation. Scale bars, 5 µm.

665

666

667

668

669

670

671

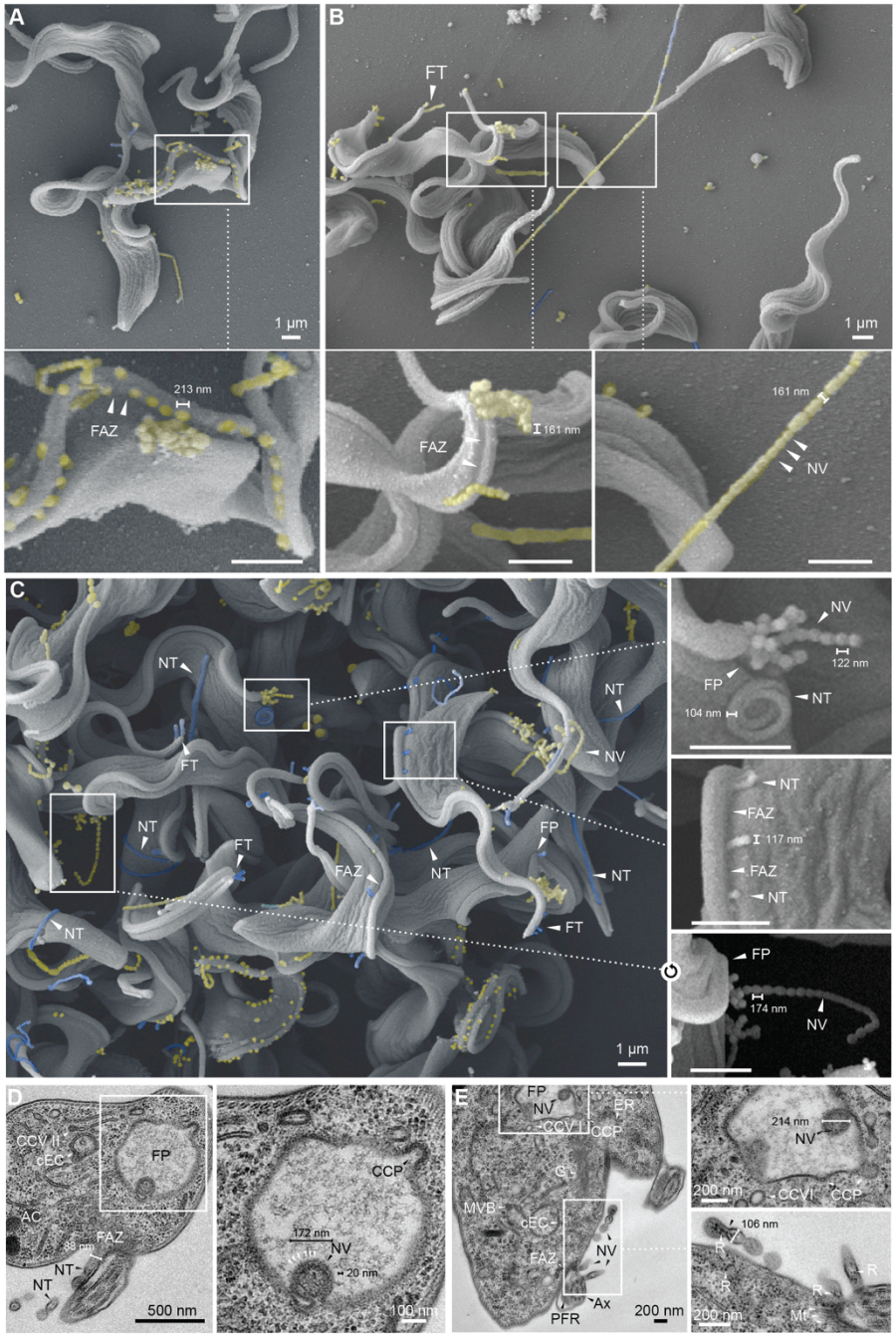

672

673

674 **Figure 6. Nanobody Treatment Triggers Formation of Nanovesicles and Nanotubes**

675 **(A-C)** Scanning electron micrographs of trypanosomes treated with a 1.7-fold molar excess of

676 $NB11_{VSG2}$ compared to VSG monomer present. FT, flagellar tip; FAZ, flagellar attachment zone;

677 NV, nanovesicle; NT, nanotube; FP, flagellar pocket. Cells treated for only 2 min **(A,B)**

678 displayed nanovesicles (yellow) as well as some chains of nanovesicles (yellow) with diameters
679 of around 200 nm. Nanotube-like structures (blue) of slightly smaller diameter and lengths
680 exceeding 1 µm could also be observed. All structures emanated from around the FAZ, FT and
681 PP. Cells treated for 10 min **(C)** show an increased and roughly equal abundance of both
682 nanovesicles and nanotubes suggesting them to be independent structures.

683 **(D,E)** TEM images of chemically fixed VSG2 expressing cells treated with a 1.7-fold molar
684 excess of $NB11_{VSG2}$ compared to VSG2 monomer present. CCVII, clathrin coated vesicle II;
685 cEC, circular exocytic carrier; FP, flagellar pocket; AC, acidocalcisome; FAZ, flagellar
686 attachment zone; NT, nanotube; NV, nanovesicle; CCP, clathrin coated pit; ER, endoplasmic
687 reticulum; CCVI, clathrin coated vesicle I; G, Golgi; MVB, multivesicular body; PFR,
688 paraflagellar rod; Ax, axoneme; Mt, mitochondrion; R, ribosome. **(D)** Concomitant formation of
689 a nanovesicle in the flagellar pocket and a nanotube from the proximity of the flagellar
690 attachment zone (FAZ). Formation of a clathrin coated pit in the FP is also apparent and suggests
691 the endocytic pathway to be functional. The budding NV has approx. 20 nm thick structures
692 coating the outer membrane consistent with the length of VSG molecules. **(E)** Concomitant
693 formation of a nanovesicle in the flagellar pocket and nanotubes from the proximity of the FAZ.
694 Nanovesicles can form chains with continuous content and contain electron-dense particles that
695 resemble ribosomes found in the cytoplasm.
696
697
698
699
700

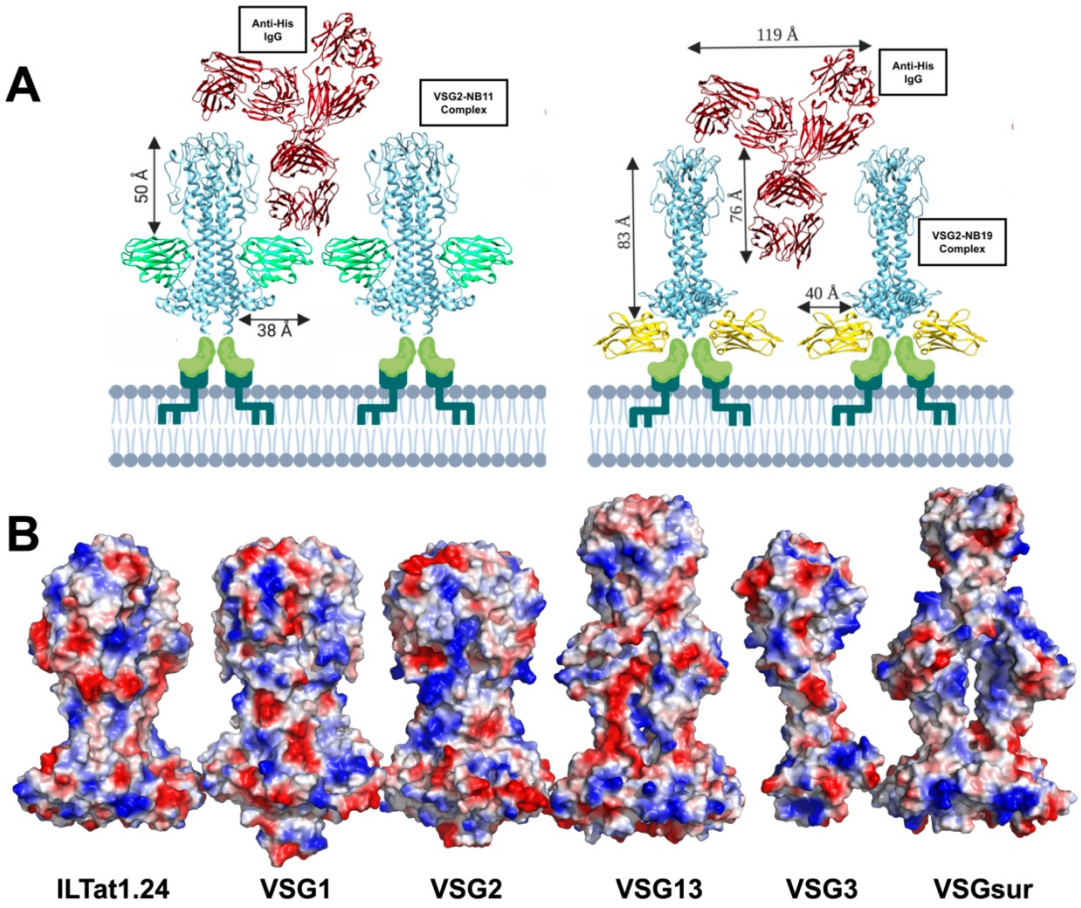

Figure 7. Nanobodies Provide a "Molecular Ruler" to Gauge VSG Accessibility

(A) Schematic of the interaction of an anti-His monoclonal IgG antibody with the VSG coat during FACS experiments. The trypanosome membrane is shown at the bottom with idealized lipids into which the (dark green) GPI anchor of the C-terminal domain (medium green) inserts. Above that is a ribbon diagram drawing of a VSG2 dimer (cyan) with a bound Nb ($NB9_{VSG2}$, $NB11_{VSG2}$, $NB14_{VSG2}$ superimposed in light green, left) or $NB19_{VSG2}$ (yellow, right). The IgG is shown as a ribbon diagram colored red (PDB ID 5DK3). **(B)** Panel of crystal structures of VSGs drawn as molecular surfaces colored by relative electrostatic potential (blue is positive/basic, red is negative/acidic, and white is neutral). RCSB PDB IDs for models used are ILTat1.24 (2VSG), VSG1 (5LY9), VSG2 (1VSG), VSG13 (6Z8H), VSG3 (6ELC), and VSGsur (6Z7A).

712 Molecular graphics software used: Chimera (Pettersen et al., 2004), CCP4mg (McNicholas et al.,
713 2011), and biorender.com Pro.
714
715
716
717
718
719
720
721
722
723